Medical & Biological Engineering & Computing
https://doi.org/10.1007/s11517-023-02901-3

ORIGINAL ARTICLE

# Microstructural fatigue fracture behavior of glycated cortical bone

**Ebrahim Maghami**[1] · **Ahmad Najafi**[1]

Received: 15 January 2023 / Accepted: 29 July 2023


**Abstract**
The current study aims to simulate fatigue microdamage accumulation in glycated cortical bone with increased advanced glycation end-products (AGEs) using a phase field fatigue framework. We link the material degradation in the fracture toughness of cortical bone to the high levels of AGEs in this tissue. We simulate fatigue fracture in 2D models of cortical bone microstructure extracted from human tibias. The results present that the mismatch between the critical energy release rate of microstructural features (e.g., osteons and interstitial tissue) can alter crack initiation and propagation patterns. Moreover, the high AGEs content through the increased mismatch ratio can cause the activation or deactivation of bone toughening mechanisms under cyclic loading. The fatigue fracture simulations also show that the lifetime of diabetic cortical bone samples can be dependent on the geometry of microstructural features and the mismatch ratio between the features. Additionally, the results indicate that the trapped cracks in cement lines in the diabetic cortical microstructure can prevent further crack growth under cyclic loading. The present findings show that alterations in the materials heterogeneity of microstructural features can change the fatigue fracture response, lifetime, and fragility of cortical bone with high AGEs contents.

**Keywords** Fatigue fracture · Cortical bone · Glycation · Critical energy release rate · Phase field fracture

## 1 Introduction

Bone with its hierarchical structure is the main load-bearing tissue of human body. With excessive loading, bone undergoes failure. One common cause of bone failure is fatigue [1, 2]. The mechanisms related to crack formation under cyclic loading are widely found in bone fracture. Fatigue fracture is associated with injuries in individuals engaged in marching or running regime and the elderly by habitual daily loading [3–6]. Fatigue fracture is influenced by various factors in human bone such as loading history, bone repair mechanisms, and diseases associated with alterations in bone mass and quality [1].

In healthy bone, the rate of microdamage accumulation is slow during cyclic loading and there is sufficient time for bone to activate repair mechanisms [7, 8]. However, a high rate of microdamage accumulation and decreased healing rate result in catastrophic failure [9, 10]. With age-related and bone-fragility diseases such as diabetes, different factors such as changes in bone mass and quality at different length scales can affect the accumulation of damage. In diabetes, one of the important alterations in bone tissue is the high accumulation of advanced glycation end-products (AGEs) due to non-enzymatic glycation [11]. AGEs content increases in bone tissue with aging [12]. The increased content of AGEs can affect the mechanical properties and fracture response of bone tissue [13]. For instance, high contents of AGEs can result in a reduction in fracture toughness of human cortical bone [14], and an increase in microdamage accumulation in the bone microstructure [15, 16].

There are various studies on the impact of AGEs on bone tissue; however, there are no in-depth discoveries yet on how the human bone microstructure with a high level of AGEs behaves under cyclic loading. To investigate the mechanisms of fatigue-driven crack growth at the microscale level, numerical fracture frameworks can assess the impact of various parameters (e.g., material heterogeneity and mismatch) on the fracture behavior of bone with high AGEs levels. Using computational tools, various studies evaluated the fracture response of bone under cyclic loading. For instance, a study has modeled cracks propagation in bone using the eXtended finite element method (XFEM), and it has been shown that there is a decrease in the stress amplitude for fail-

✉ Ahmad Najafi
arn55@drexel.edu

[1] Drexel University, Philadelphia, PA, USA

Published online: 16 August 2023

ure with aging by fatigue crack initiation analyses [17]. In another study, the effects of various factors such as age and gender on the rate of damage accumulation have been evaluated using a finite element model [18]. In another work, a neural network model has been combined with a finite element method to predict bone fatigue crack growth [19]. In addition, another study has evaluated the micromechanics of the cement-bone interface under tensile fatigue loading by finite element method to discover the role of the underlying mechanisms in the fatigue behavior of this interface [20].

It should be noted that crack growth simulation in highly heterogeneous materials is numerically difficult [21]. This is due to the complexity of the multiple unpredictable branching and merging cracks during fracture processes. To model crack growth, there are different numerical methods using discrete approaches such as the cohesive zone approach developed by Remmers et al. [22], XFEM presented by Moees et al. [23], and the extended isogeometric method by Ghorashi et al. [24]. Such discrete approaches can simulate the crack growth path; however, there are some difficulties with crack branching or multiple crack fronts during fracture simulation processes [25]. Over the past decade, the phase field method has provided a better solution for crack initiation and propagation. In this diffuse method, it is not required to define the crack surface, and the difficulty of crack tracking is improved [26]. In this proposed approach, the surfaces of cracks are defined by a diffuse zone and are formulated by an energy degradation method to simulate damage initiation and propagation [27]. There is relatively less numerical instability in this diffuse method compared to XFEM and continuum damage mechanics [28]. Unlike continuum damage mechanics, the phase field method can control the thickness of the damage zone by a length scale parameter [29]. In contrast to XFEM, the phase field method can handle the numerical difficulties for the formation of cracks surface with multiple cracks initiation and branching ahead [21].

In addition, the phase field method has been used in different applications in the literature [21]. For instance, the phase field approach has been utilized to predict the crack growth in a new physics informed neural network (PINN) scheme [30]. Furthermore, a phase field method is used to evaluate the influence of the interface zones on fracture response in the polymeric nanocomposites (PNCs) [31]. Additionally, this diffuse approach has been utilized to evaluate the fracture behavior of various materials such as human bone and dentin [32–37], brittle biomaterials [38], and polymeric nanocomposites [31].

In the present work, we study the micromechanisms of fracture in cortical bone with a high level of AGEs under cyclic loading. We consider that the material properties of bone are subjected to change due to the high content of AGEs by reducing the fracture toughness of bone. To model the initiation and propagation of cracks in bone, we develop a phase field method to simulate fatigue fracture.

## 2 Materials and methods

### 2.1 Preparing human cortical bone samples

Using two cadaveric female human tibias (ages: 60 and 81), we cut the cross-section at 50% of the mid-shaft length in each tibia to extract samples (as shown in Fig. 1). The two tibias are collected from a donor bank (Anatomy Gifts Registry, Hanover, MD). The samples collection, ethical approval, and bone sample preparation are performed in and gained by the Bone Biomechanics Lab at UMass Dartmouth. We also carry out a silver-nitrate staining technique on 8 $\mu$m thick sections from the samples to have a more clear visualization of microstructural features such as cement lines (Fig. 1b). Further details on the sample preparation and staining technique can be found in the other works [33, 34, 39]. In the next step, with a microscope, we take microscopy images from the anterior and posterior regions of the 60- and 81-year-old cortical bone samples (Fig. 1d). With the help of a random algorithm, we choose three different 1-$mm^2$ areas in all anterior and posterior samples for each age.

### 2.2 Constructing 2D finite element models

We use the microscopy images to create two-dimensional (2D) models. With a manual segmentation method, we determine the boundaries of osteons and Haversian canals. We create the 2D plane strain models by importing the geometrical data from the segmentation to Abaqus (Fig. 1e). Our assumption for plane strain condition can be justified by considering the higher size of longitudinal direction in the tibia compared to its average transverse dimensions. Thus, the strains values in the longitudinal direction are far lower than strains in the transversal direction. In addition to that, the length of the whole tibia is not affected by the transversal loading condition in the models. These assumptions are in agreement with other works [40–42]. The thickness of all cement lines is considered to be 5 $\mu$m in all models. We also create the homogenized area in each model with a thickness of 0.05 mm on the four sides of the bone sample to prevent any boundary condition effects. Thus, the dimensions of the 2D models are 1.1 mm by 1.1 mm. All models also have a precrack with a length of 0.05 mm (Fig. 1c).

### 2.3 Mechanical properties of microstructural features

Table 1 shows the mechanical properties of the 60-year-old samples. We adopt the data reported by Fan et al. [43] to

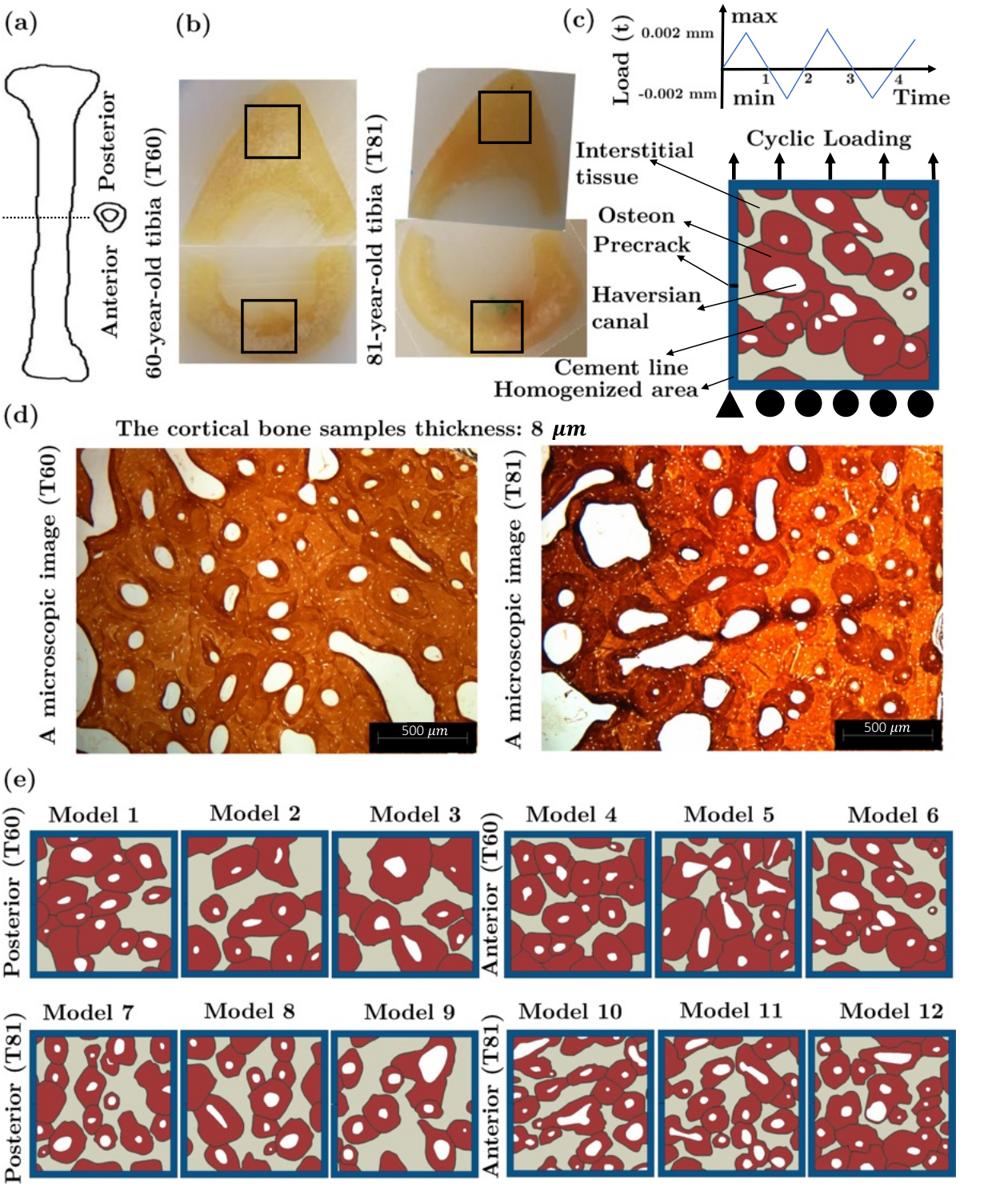


**Fig. 1** **a** A human tibia is schematically shown, **b** the extracted cross-sections from the cortical 81- and 60-year-old samples, **c** the loading and boundary conditions on all models with a cyclic loading condition with a minimum load of −0.002 mm and a maximum load of 0.002 mm with a time period of 2 s, **d** two examples of microscopy images taken from the samples after the staining technique, and **e** the 2D models constructed from the microscopy images

**Table 1** Mechanical properties of cortical features for the 60-year-old samples: critical energy release rate ($G_c$), Young's modulus ($E$), and Poisson's ratio ($v$) for osteons, interstitial tissue, cement lines, and homogenized tissue

| Material property | Osteon | Interstitial tissue | Cement lines | Homogenized tissue |
|---|---|---|---|---|
| $G_c$ (N/mm) | 0.62[(2)] | 0.52[(2)] | 0.1629[(2)] | 0.57[(2)] |
| E (GPa) | 16.6[(1)] | 19.7[(1)] | 12.45[(4)] | 18.15[(5)] |
| $v$ | 0.25[(3)] | 0.25[(3)] | 0.3[(5)] | 0.25[(3)] |

(1) [43];(2) [46]; (3) [60]; (4) [42, 61], and [62]; (5) [45]

find elastic moduli of osteons and interstitial tissue by calculating the average of the data in the radial orientation. Our assumption for $G_c$ of osteons and interstitial tissue is that their $G_c$ values are inversely proportional to the values of their elastic moduli. This is justified by the information that calcified tissues (e.g., bone) with a high stiffness have a lower toughness [44]. The elastic modulus of cement lines is also assumed to be 25% lower than that of osteons. $G_c$ of the cement lines is calculated based on an average value from the work of Giner et al. [45]. Additionally, the mechanical properties of the homogenized region are found based on the average values of osteons and interstitial tissue. All material properties in this study are homogeneous and isotropic. Using the mechanical properties presented in Table 1 as the base data, we find the material properties of the 81-year-old samples with a function between age and the material properties suggested by Brown et al. [46].

## 2.4 The relationships between AGEs and $G_c$

With aging, AGEs levels in human cortical bone can be elevated and a relationship suggested by Tang et al. [47] shows how the decreased energy release rate ($G_c$) is in correlation with the increased concentration of AGEs:

$$\Delta_{G_c} = 20.979 Ln(\Delta_{AGEs}) - 65.734. \quad (1)$$

Here, based on the relationship in Eq. 1, our assumption is that the elevated AGEs in the 60-year-old and the 81-year-old samples can reduce the $G_c$ of their osteons, interstitial tissue, and cement lines. To simulate the role of the increased AGEs in the cortical bone models, we assume three possible cases for the reduction in $G_{ost}$ and $G_{int}$ with an increase in AGEs concentration (shown in Table 2). We also assume that the three possible cases show different mismatch ratios ($R_g$) between $G_c$ of osteons and interstitial tissue. The mismatch ratio is defined such that $R_g = \frac{G_{ost} - G_{int}}{G_{ost}} \times 100\%$.

## 2.5 Computational sets

(i) In the first set of simulations, we analyze crack growth trajectories in the anterior and posterior regions of the 81- and 60-year-old under cyclic loading. The cyclic loading condition is considered to be with a minimum load ($U_{min}$) of $-0.002$ mm and a maximum load ($U_{max}$) of 0.002 mm with a time period of 2 s with a loading range ($\Delta U = U_{max} - U_{min}$) of 0.004 mm. In this set of simulations, the purpose is to compare the fracture response and lifetime (N, the number of cycles before the complete fracture of the sample when its loading capacity drops to zero) of the 81- and 60-year-old models. Thus, all simulations in this set are under the same cyclic loading condition.

(ii) In the second set, we analyze the fracture behavior of each model presented in Fig. 1e, considering each case of the mismatch ratio as presented in Table 2 under the cyclic loading. Here, we aim to investigate the influence of changing the mismatch ratios on the lifetime and crack growth trajectories in each model. We further compare the results of one region with another region. We implement the same cyclic loading condition explained in the previous set.

(iii) In the last set, we find the influence of increasing and decreasing the loading range ($\Delta U = U_{max} - U_{min}$) on the lifetime of Model 1. We use the same cyclic loading condition in Set (i).

**Table 2** Three possible values for the mismatch between $G_{ost}$ and $G_{int}$ at the level of 100% increase in AGEs

| Loss in critical energy release rates of osteons and interstitial tissue (%) | Mismatch ratio between $G_{ost}$ and $G_{int}$: $R_g = (\frac{G_{ost} - G_{int}}{G_{ost}}) \times 100\%$ |
|---|---|
| 20% loss in $G_{ost}$ and 70% loss in $G_{int}$ | $R_g = 70\%$ |
| 30% loss in $G_{ost}$ and 60% loss in $G_{int}$ | $R_g = 50\%$ |
| 45.5% loss in both $G_{ost}$ and $G_{int}$ | $R_g = 15\%$ |

$R_g$ indicates the mismatch ratio in each case

### 2.6 Presenting a phase field framework for fatigue fracture

In the current work, we use a phase field method developed by Miehe et al. [27] to simulate crack initiation and propagation in cortical bone. To analyze model crack growth trajectories in this diffusive approach, the minimization term of an energy functional for a material is

$$\Pi^{int} = E(\boldsymbol{u}, d) + W^{dmg}(d), \tag{2}$$

where $\Pi^{int}$, $E(\boldsymbol{u}, d)$, and $W^{dmg}(d)$ are the total potential energy, the elastic energy in the body, and the required energy for the formation of cracks surface, respectively. d∈ [0,1] defines the damage field variable in the material such that the unbroken state of the material is $d = 0$ and the broken state is $d = 1$. $\boldsymbol{u}$ in Eq. 2 represents the displacement field in the material.

In the damaged material, the elastic energy is introduced such that

$$E(\boldsymbol{u}, d) = \int_{\Omega} \Psi(\boldsymbol{\varepsilon}(\boldsymbol{u}), d)\, d\Omega, \tag{3}$$

where $\Psi(\boldsymbol{\varepsilon}(\boldsymbol{u}), d)$ and $\boldsymbol{\varepsilon}(\boldsymbol{u})$ are the strain energy density and the symmetric strain tensor, respectively. The work of Miehe et al. [27] presents more details on the stress tensor and the degraded strain energy.

The required work for crack formation in Eq. 2 without considering fatigue fracture, $W^{dmg}(d)$, takes the form such that

$$W^{dmg}(d) = \int_{\Omega} G_c\, \gamma(d, \nabla d)\, d\Omega, \tag{4}$$

where $G_c$ is the critical energy release rate. The crack density function, $\gamma(d, \nabla d)$ presented by Bourdin et al. [48], is defined such that

$$\gamma(d, \nabla d) = \frac{1}{2l_c} d^2 + \frac{l_c}{2}\, \nabla d \,.\, \nabla d, \tag{5}$$

where $l_c$ is the length scale parameter. This parameter defines the thickness of the damaged zone between the unbroken and broken states of the material (the thickness of the crack).

To solve the problem, we define the energy functional for the displacement field problem such that

$$\Pi^{u} = \int_{\Omega} (\Psi(\boldsymbol{\varepsilon}(\boldsymbol{u}), d) - \bar{\boldsymbol{b}}.\boldsymbol{u})\, d\Omega - \int_{\partial\Omega} \bar{\boldsymbol{t}}.\boldsymbol{u}\, d\partial\Omega. \tag{6}$$

To implement fatigue fracture in the phase field framework, we use a theoretical framework for brittle materials based on the work of Kristensen et al. [49]. In this framework, the energy functional of the phase field problem (the crack problem) takes the form

$$\Pi^{d} = \int_{\Omega} \left( f(\bar{\lambda}(t))\, G_c\, \gamma(d, \nabla d) + (1 - d^2)\, \mathcal{H} \right) d\Omega, \tag{7}$$

where $\mathcal{H}$ defines strain history functional to satisfy the irreversibility of the crack propagation and is the connection between the displacement and phase fields. $f(\bar{\lambda}(t))$ is assumed to be a fatigue degradation function and is dependent on a variable $\bar{\lambda}(t)$ known as a cumulative history [49–51]. $t$ is also the time variable over a cyclic loading.

The cumulative history $\bar{\lambda}(t)$ can be defined such that

$$\bar{\lambda}(t) = \int_{0}^{t} \Theta(\lambda\dot{\lambda})\, dt, \tag{8}$$

where $\Theta(\lambda\dot{\lambda})$ is the Heaviside function. $\lambda$ is the fatigue history variable and denotes the loading condition and $\dot{\lambda}$ is its rate. In this framework, $\lambda$ takes the form $(1 - d)^2 \Psi_0^+$ where $\Psi_0^+$ is the positive part of the elastic energy of the uncracked material [50]. Furthermore, the fatigue degradation function $f(\bar{\lambda}(t))$ accounts for the sensitivity of the required work for the formation of crack surface with respect to the number of cycles

$$f(\bar{\lambda}(t)) = \begin{cases} 1 & if \quad \bar{\lambda}(t) < \lambda_{th} \\ 2\lambda_{th} / (\lambda_{th} + \bar{\lambda}(t)) & if \quad \bar{\lambda}(t) \geq \lambda_{th} \end{cases} \tag{9}$$

where $\lambda_{th}$ is a value that serves as a threshold below which the fracture energy is not affected. This threshold is assumed to be $\lambda_{th} = G_c \,/\, 12 l_c$ [49]. Further details on instructing the variations of the two energy functionals presented in Eqs. 7 and 6, the implementation of fatigue degradation function, deriving the strong forms, and finite element discretization can be found in the works of Alessi et al. [50] and Kristensen et al. [49].

To solve the phase field and displacement problems, we implement a quasi-Newton monolithic technique in a user-defined element subroutine (UEL) into Abaqus developed by Kristensen et al. [49]. We generate four-node elements for all 2D models. The numbers of elements are approximately between ~600,000 and ~800,000 in all models. In addition, we perform mesh convergence tests for all models. As presented in Fig. 1, we apply the cyclic displacement loading as described in Sect. 2.5 on the top edge of the 2D models. The fixed bottom edge along the $y$ direction and the fixed bottom left corner along the $x$ and $y$ directions are the constraints for the boundary conditions (shown in Fig. 1). The length scale parameter in all models is $l_c$ = 0.001 mm presenting the damaged (phase field) zone thickness (5).

## 3 Results

In this section, we report the activation or deactivation of toughening mechanisms in the cortical bone samples with increasing mismatch ratio due to elevated AGEs and compare the fracture responses of the 60- and 81-year-old models under cyclic loading.

Figure 2 depicts the fracture behavior of the models (Models 1–12 shown in Fig. 1e) under the same cyclic loading as presented in Sect. 2.5. With the results of Fig. 2, we compare the fracture response of the models from one age (60) to another (81). We observe various crack growth trajectories and toughening mechanisms in Fig. 2 such as crack deflection, crack merging, microcracking, and crack propagation in cement lines. In this context, the majority of the microcracks formation are located around the Haversian canals (Fig. 2). The formation of microcracks around the Haversian canals is not dependent on the size of the canals, and it

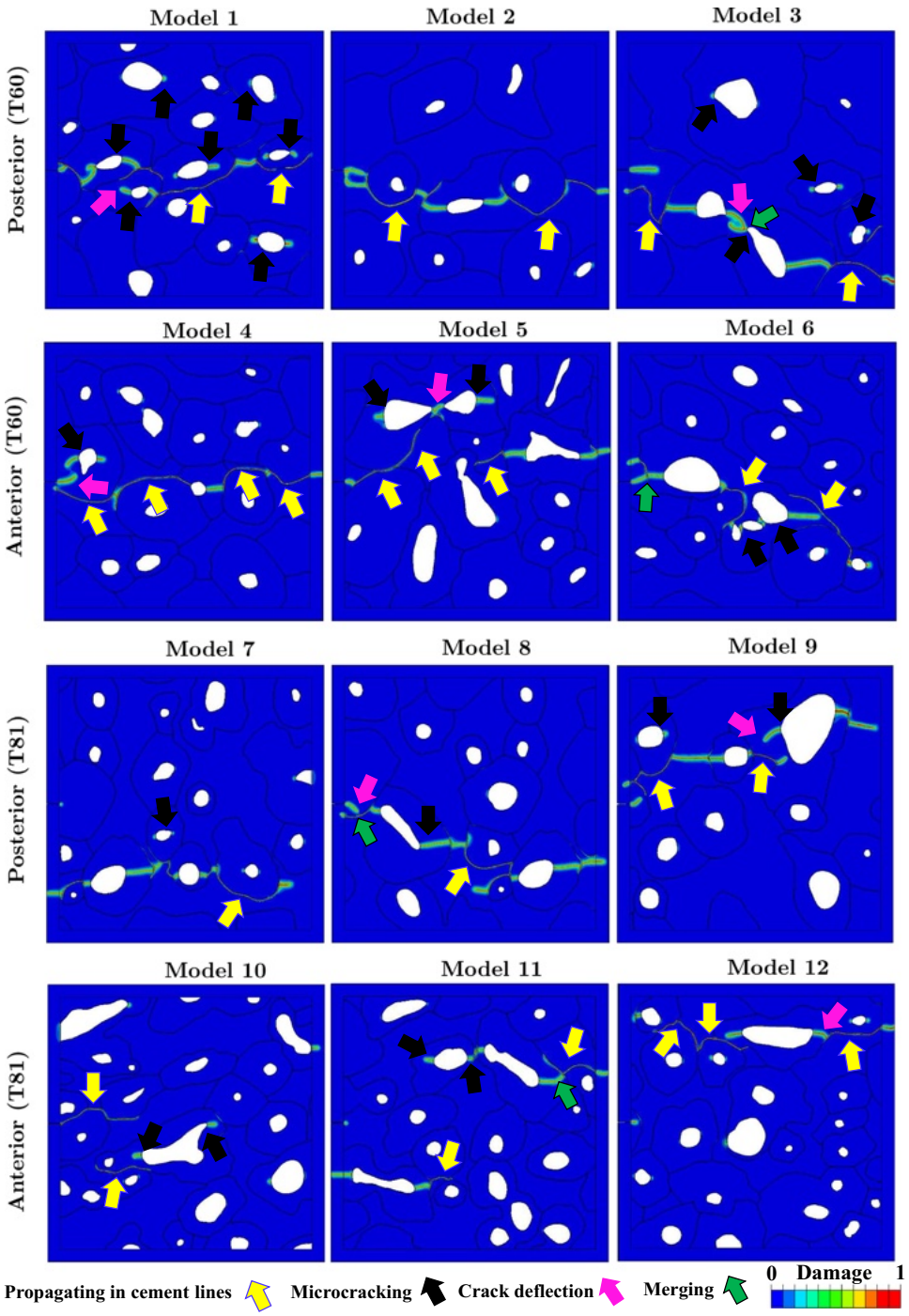


**Fig. 2** The fracture results of the 2D models (Models 1–12) in Fig. 1e under the same cyclic loading in Sect. 2.5. Various fracture mechanisms occur such as crack deflection, cement lines debonding, microcracking, and crack merging

occurs around small and large canals (Fig. 2). Another role of the canals is that they can attract and deflect the main cracks from their original path due to their high-stress concentration. Crack propagation in cement lines is another mechanism in the simulations in Fig. 2. We observe that after the main crack penetrates the cement lines it grows a long curvy path, which can be seen in some of the simulations such as Models 4 and 5. This mechanism prevents cracks from breaking the whole osteons. Another crack growth mechanism is crack deflection. The simulations indicate that cracks can deviate toward the microcracks and the canals ahead (Fig. 2). This can cause the cracks to not stay on the straight path anymore. The deflected cracks are eventually merged with other cracks or microcracks as shown in Fig. 2.

Figure 3a also presents the lifetime fraction ($N/N_R$ where $N_R$ is 100 cycles) of all fractured models depicted in Fig. 2. Models 4 and 5 have a lower number of cycles until failure than the rest of the models (Fig. 3a). For Model 4, the reason is that the crack penetrates into the cement lines and propagates in an almost continuous path of the cement lines in the whole sample. Thus, the crack grows in the entire sample without being delayed by any activated toughening mechanisms ahead. However, for Model 5, there are multiple crack formations around different large canals and this causes a reduction in the resistance of the model to fracture. In Model 5, the first microcrack initiates from the Haversian canal and merges with another microcrack (Fig. 3e). Other microcracks are also formed from some other Haversian canals (Fig. 3e).

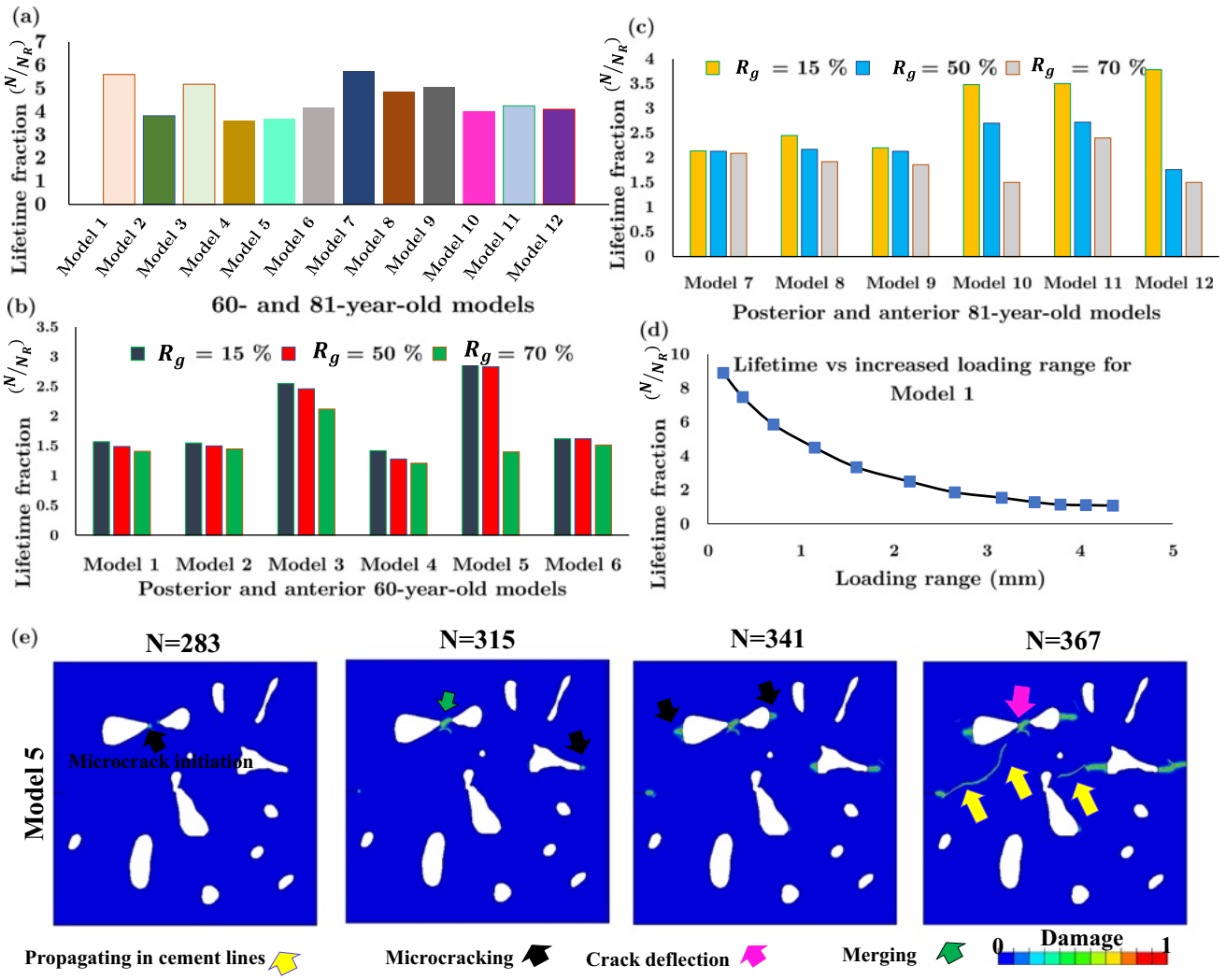


**Fig. 3** **a** The lifetime results (N) of all models presented in Fig. 2d under the same cyclic loading in Sect. 2.5. $N_R$ is 100 cycles. The number of cycles for the results of three $R_g$ ratios for each model of **b** the 60-year-old samples and **c** the 81-year-old samples, and **d** the lifetime fraction of Model 1 versus increasing loading magnitude. **e** It shows the crack trajectory in Model 5 as an example to demonstrate how microcracks initiate and propagate during the lifetime and the number of cycles for each snapshot from the progress

In addition, another crack nucleates from the precrack and propagates into the cement lines (Fig. 3e). Moreover, Models 1 and 7 have the highest lifetime fraction ($N/N_R$) among all models (Fig. 3a). The reason for Model 1 is while the main crack propagates in the cement lines, different toughening mechanisms such as microcracking and crack deflection (Fig. 4) are simultaneously activated in the sample. Thus, the activation of these mechanisms causes a delay in crack propagation and it requires more time for the cracks to reach that level of energy to break out of the cement lines trap. Additionally, for Model 7, the geometry is formed in such a way (more separated osteons and not formed a large osteonal area ahead of cracks) to delay the initiation of cracks from the canals based on the reverse cyclic loading. It should be noted that there is a drop in the lifetime of all samples in Fig. 3b and c (where different mismatch ratios are considered) compared to the lifetime of the same samples in Fig. 3a (where no mismatch ratios are considered in the simulations). This reduction in lifetime is due to the drop in $G_c$ of the samples in Fig. 3b and c with increased AGEs.

Figures 4 and 5 show the fracture response of the 60-year-old posterior models (Models 1–6) considering three different mismatch ratios ($R_g = \frac{G_{ost}-G_{int}}{G_{ost}} \times 100\%$) under the same cyclic loading as described in Sect. 2.5. To investigate the influence of changing the mismatch ratio (due to increased AGEs) on the fracture behavior, we look into possible differences in the fracture results of each model with itself for three cases $R_g$ as well as changes in the number of cycles as shown in Fig. 3b. The simulations show that changes in the mismatch ratio do not significantly affect the crack growth trajectories in Model 1, and it eventually results in a few changes in the number of cycles. In Model 2, we observe a few microcracks by decreasing the mismatch ratio (Fig. 4). This results in a decreased number of cycles to complete failure, as there are not enough microcracks surrounding the main crack to delay the crack propagation. The results in

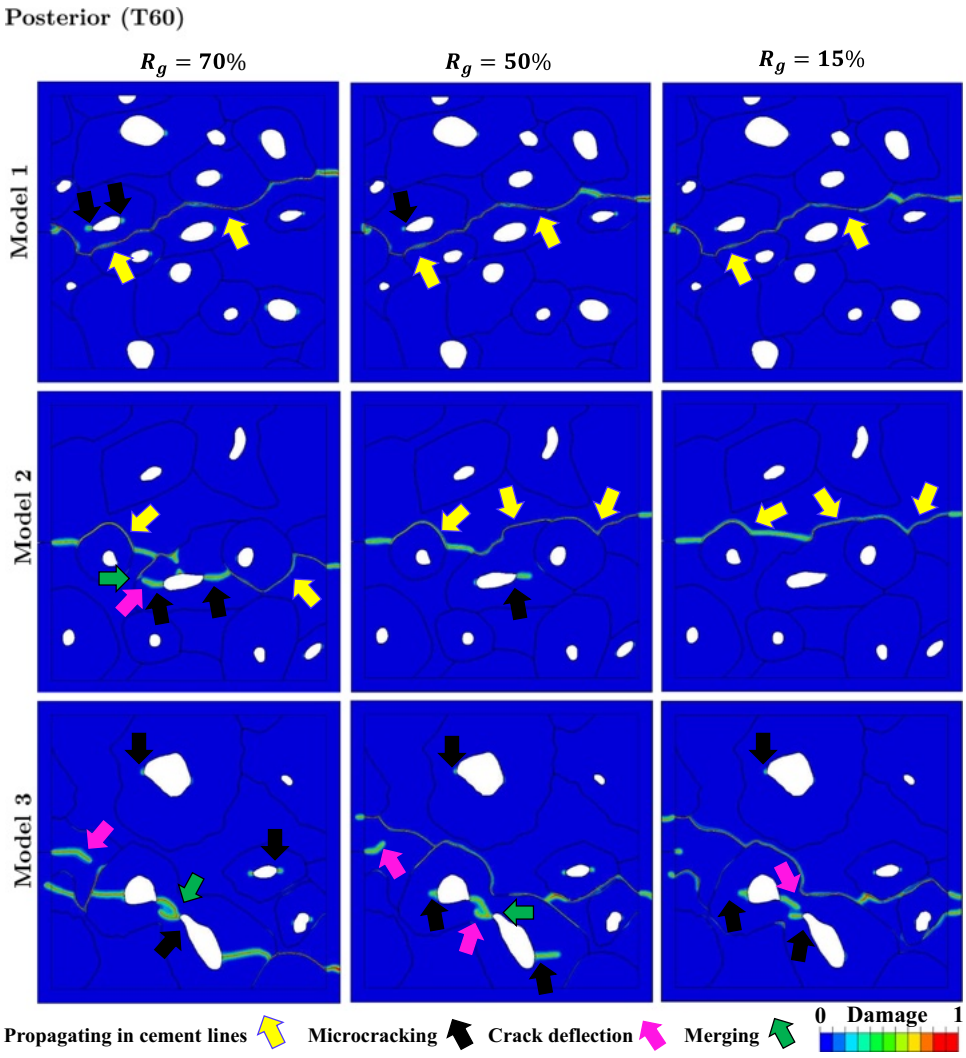


**Fig. 4** The fracture response of the posterior models of age 60 (Models 1–3) in Fig. 1e under the same cyclic loading as described in Sect. 2.5. The fracture results of three $R_g$ ratios (introduced in Table 2) are shown for each model

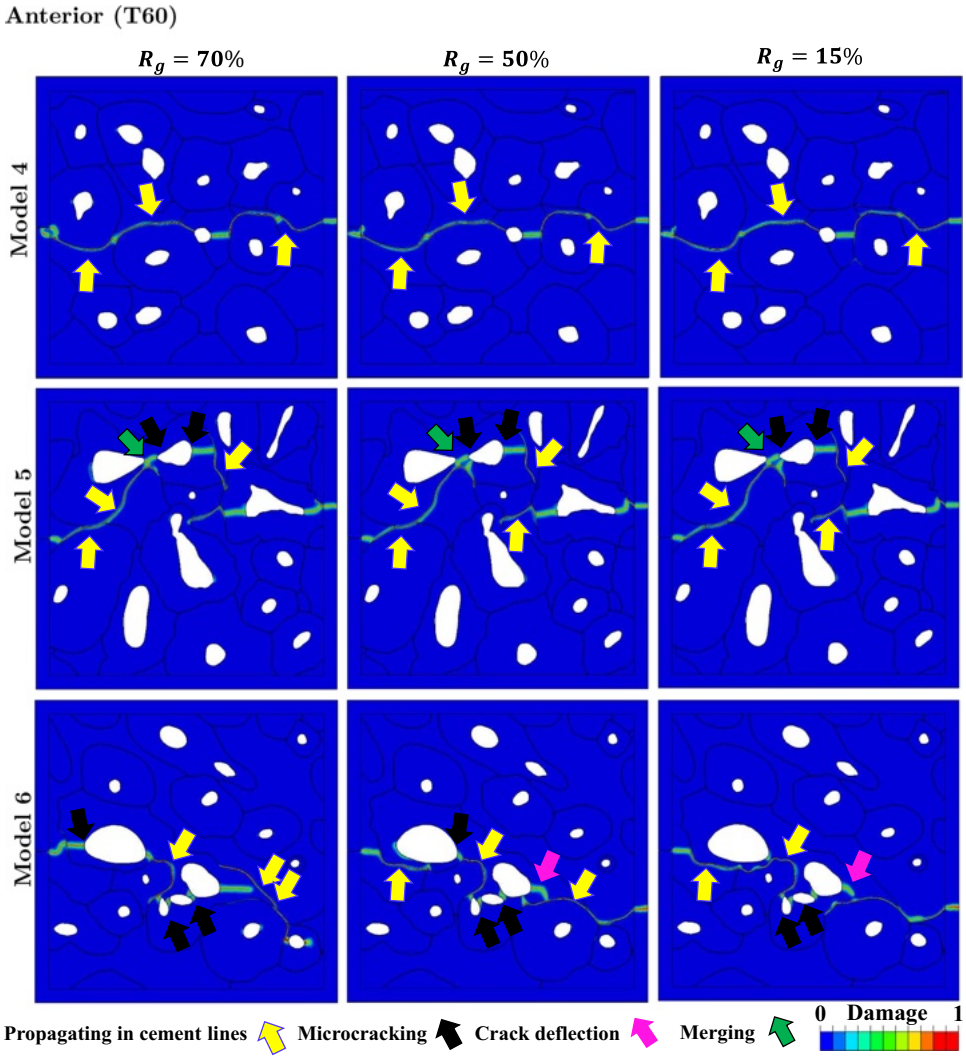


**Fig. 5** The fracture results of the anterior models of age 60 (Models 4–6) in Fig. 1e under cyclic loading. Different mechanisms are activated under $R_g$ ratios (shown in Table 2)

Model 3 show the formation of the crack is dependent on changes in the mismatch ratio by increasing or decreasing the accumulation of damaged cement lines (Fig. 4). The highest mismatch case in Model 3 has a lower number of cycles than the rest of the cases, and this might be due to a lower damage accumulation in cement lines in the highest mismatch case.

Additionally, in Models 4 and 5 as shown in Fig. 5, we observe that there are not many differences in the crack propagation patterns. In Model 4, there is a long connection of cement lines, and the main crack is trapped by them, which eventually results in negligible changes in the number of cycles by changing the mismatch ratio (Fig. 3b). In Model 5, there are multiple large canals that microcracks can easily initiate around them (Fig. 5). This can result in a drop in the lifetime of Model 5 in the case that there is a high mismatch between the properties of osteons and interstitial tissue ($R_g$= 70% in Fig. 3b). In Model 6, we observe more damaged cement lines by decreasing the mismatch ratio. Those damaged cement lines in the $R_g$= 50% and 15% cases for Model 6 provide a path that cracks cannot grow in osteons ahead and resulting in a higher lifetime compared to the highest mismatch case ($R_g$= 70%) where cracks propagate in osteons.

Figures 6 and 7 depict the fracture behavior of the 81-year-old anterior models (Models 7–12) under the same cyclic loading as described in Sect. 2.5 by considering three different mismatch ratios ($R_g = \frac{G_{ost}-G_{int}}{G_{ost}} \times 100\%$). In Model 7, there are no considerable changes in the crack growth trajectories by increasing the mismatch ratio (Fig. 6). This results in a negligible reduction in the lifetime with the increased mismatch ratio (Fig. 3c). In Model 8, we observe more damage propagation in cement lines by decreasing the mismatch ratio $R_g$ (Fig. 6), and this causes less damage accumulation in osteons and the interstitial matrix resulting in an increase in the lifetime (Fig. 3c). In Model 9, the crack growth pattern is not affected by altering the mismatch ratio. However, the lifetime is decreased for the case $R_g$= 70% due to the drop in the fracture properties of both osteons and interstitial tissues and eventually the reduced resistance for crack propagation.

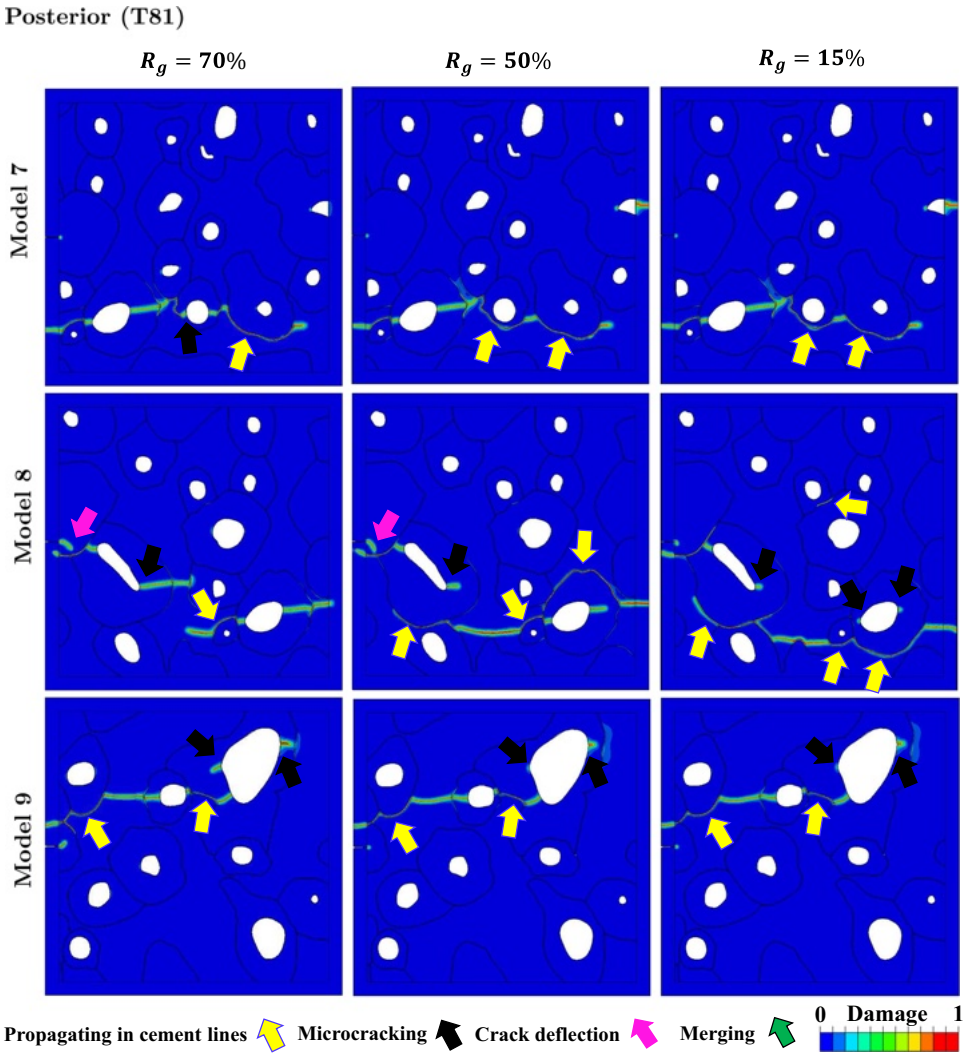


**Fig. 6** Crack growth in the posterior models of age 81 (Models 7–9) in Fig. 1e under the cyclic loading (Sect. 2.5). For each model, three $R_g$ cases are introduced (Table 2)

Additionally, in Models 10 and 12, increasing the mismatch ratio $R_g$ cannot change the crack growth trajectories (Fig. 7). With the increased mismatch ratio $R_g$, we observe a decrease in the lifetime of Model 10 (Fig. 3c). The reason for this decreased lifetime in Model 10 can be due to the low difference between the fracture properties of osteons and interstitial tissue and cracks can break easily in both tissues. However, in Model 12, negligible changes in the lifetime in the cases $R_g$= 50% and $R_g$= 15% are due to more crack propagation in the cement lines (Fig. 7) which facilitates the crack propagation, but the case $R_g$= 70% has fewer damaged cement lines and more drop in the fracture properties of the cortical microstructure and has a lower number of lifetime compared to other cases. In Model 11, crack propagation depends on the increased mismatch ratio. We observe a decrease in both damaged cement lines and the lifetime by increasing the mismatch ratio (Figs. 7 and 3c). One possible explanation for the reduced cycles is that there are more damaged osteons. In the case with the lowest mismatch ($R_g$= 15%), the cracks cannot also easily break into the osteons as there is a low drop in the fracture properties values of the tissues.

Moreover, Fig. 3d presents the changes in the lifetime of Model 1 by decreasing the amount of the cyclic load as described in Sect. 2.5. As shown in Fig. 3d, as expected, there is an increase in the number of cycles for Model 1 with decreasing the applied load.

## 4 Discussion

In the current study, we evaluate fatigue fracture of human cortical samples using a phase field framework. Here, the purpose is to understand the impact of changes in the mismatches between the microstructural properties on crack growth trajectories in cortical bone with a high level of AGEs under cyclic loading.

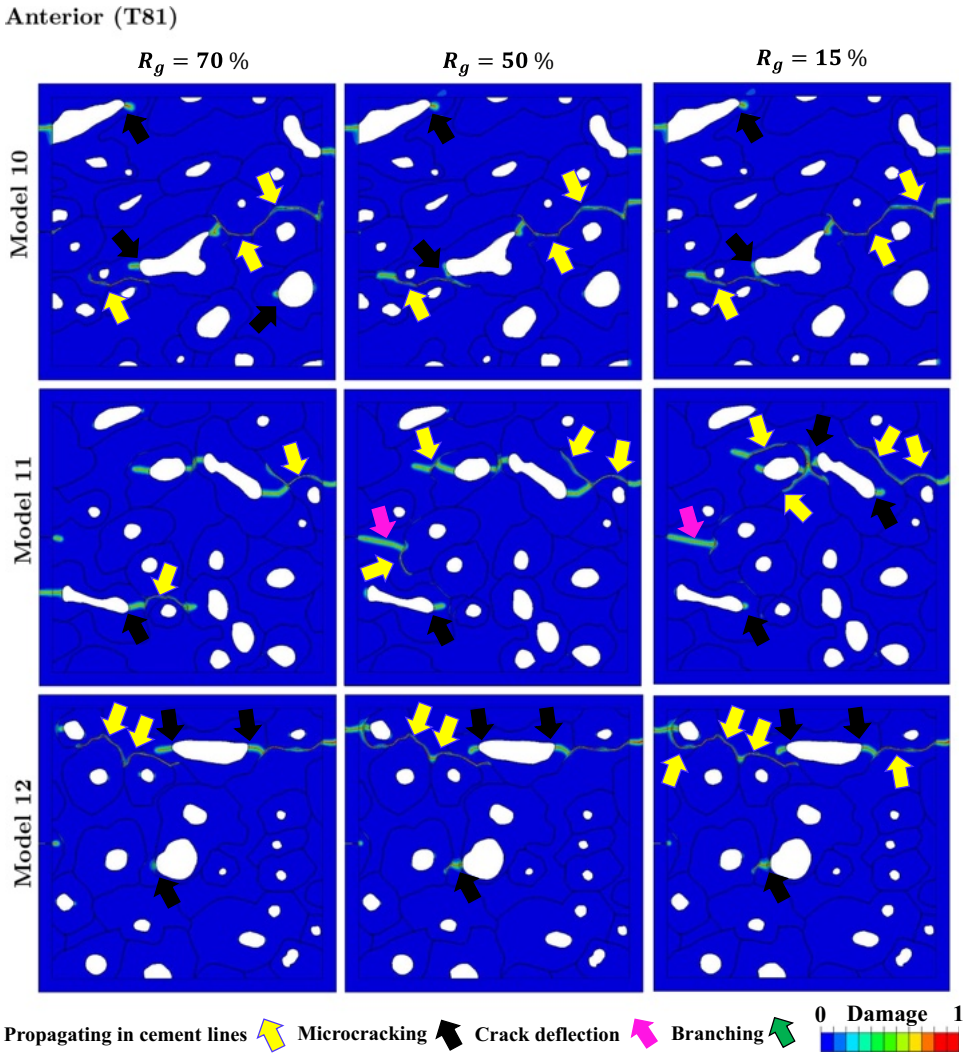


**Fig. 7** The fracture results for the anterior models of age 81 (Models 10–12) under cyclic loading. Crack trajectories are displayed for three $R_g$ ratios for each model

Another assumption that we have in the present study is AGEs accumulation can result in changes in the mismatch between the fracture properties of the microstructural features. This is in relation to changes in bone turnover due to high AGEs levels [12, 52] and the fact that the AGEs content in osteons might differ from the AGEs content accumulated in the interstitial tissue. To simulate such effects, we consider various mismatches between the energy release rates of osteons and the interstitial matrix.

To evaluate the impact of the mismatch ratios due to the high accumulation of AGEs on the fracture response of cortical bone, we report the post-yielding properties (e.g., damaged cement lines and activation of toughening mechanisms) and the lifetime of the models until failure of cortical bone such as the total damage accumulation, the accumulation of damaged cement lines, and the occurrence of different toughening mechanisms. In the results from the present simulations, we observe crack deflection, crack merging, microcracking, and crack propagation in cement lines. These crack trajectories can undergo changes or stay the same with decreasing the mismatch ratio under cyclic loading.

During cyclic loading, fatigue microdamage accumulates in cortical bone with a graduate rate [7]. The anti-fatigue structure of cortical bone provides the tissue with remarkable mechanical properties to prevent excessive growth of cracks over time [53]. In cortical bone, osteons (as fibers) are the major load-bearing component of its microstructure [54]. In the present simulations, we observe the same load-bearing behavior, especially in some of the cases with a high mismatch ratio. In addition, the discontinuity features like pores are known as stress concentrators and redistributors [55]. This is also indicated in the results of our simulations that the microcracking formation around the canals ahead of a propagating crack can rearrange the stress pattern and eventually result in an increase in the lifetime to failure.

Other mechanisms such as crack deflection also have a vital role in preventing the propagating cracks from further growth [56]. In our simulations, the cracks can be deflected

along cement lines, which can stop the cracks from further growth by blunting the crack tip. In some models, cracks can easily propagate through the connected cement lines and break the model as the required energy for the crack growth in cement lines is lower than that of osteons and interstitial tissue. All of these crack formation mechanisms can be dependent on the level of accumulated AGEs on cortical bone and the increased or decreased mismatch properties due to the AGEs accumulation.

With the elevated AGEs in bone, there is an increase in the microcrack formation [16]. This can result in a higher rate of fatigue microdamage accumulation as its direct relationship with the rate of crack initiation and propagation [53]. In addition, the lifetime of cortical bone under cyclic loading is a function of crack accumulation. The fatigue lifetime in bone is also in an inverse relationship with the Haversian porosity [57]. The present simulations show that the lifetime of some models can decrease with excessive microcracking around the Haversian canals due to the mismatch ratio related to changes in AGEs.

Furthermore, in some of the current simulations, crack growth trajectories and fatigue lifetime remain the same or have negligible differences by changing the mismatch ratio ($R_g$) because of alterations in bone turnover through the increased AGEs. A justification for these observations might be related to the arrangement of osteons and canals. These features might have been formed in such a configuration that does not allow different patterns for cracks formation under the applied cyclic loading condition. For instance, in Model 5, there are multiple large Haversian canals close to each other that dominate the crack growth pattern, which is not affected by changing the mismatch ratio. Experimental studies also report that there are some discrepancies in the impact of AGEs on the post-yielding behavior of cortical bone [14, 58]. For example, based on observations from control samples to glycated samples in cortical bone, there are no changes in the fracture initiation toughness [58]. However, in another study, it is shown that the increased AGEs have a direct impact on the decreased fracture initiation toughness in cortical bone [14]. The cause of such inconsistent reports might be related to differences in the size and geometries of the cortical features from one sample to another [59].

It is also important to note that the interaction between the pre-existing microcracks and toughening mechanisms can also have an impact on the initiation and propagation of microcracks during cyclic loading. However, some microscopy images in the present study have some pre-existing microcracks, which are not considered in the models. Additionally, the bone repair mechanisms are not included in the present models, which can consequently change the fatigue microdamage accumulation. It should also be noticed that the present 2D models cannot simulate crack propagation along the longitudinal axis of the long bone. In addition, the mismatch cases between the fracture properties of the microstructural features are limited to a few numbers in the current study, and yet there can be more uncertainties in the impact of AGEs on the properties by aging. Furthermore, the thickness of cement lines in the cortical bone samples is considered to be the same, which does not represent the reality of cortical bone microstructure. Additionally, the mechanical properties of the samples are assumed based on the data in the literature, which is not the material property of the actual sample and can affect the lifetime results.

## 5 Conclusion

The current study analyzes the effects of various mismatch ratios between the properties of microstructural features due to elevated AGEs contents on the crack growth trajectories and fatigue lifetime of cortical bone. The proposed phase field approach is a practical numerical tool to estimate the fatigue lifetime of cortical bone and simulate different toughening mechanisms under cyclic loading. Moreover, the results of this study show that the activation and deactivation of toughening mechanisms can be dependent on the mismatch ratio between the fracture properties of cortical features due to high AGEs content. In addition, in studies on fatigue fracture of cortical bone with increased AGEs, the configuration of the microstructural features (e.g., shape and size of osteons) should be included in the fracture analyses. Furthermore, the fatigue lifetime of cortical samples can depend on the Haversian canals size and the degraded materials properties due to increased AGEs.

**Acknowledgements** The authors acknowledge the high-performance computing resources (Picotte: the Drexel Cluster) and support at Drexel University. We are grateful to Timothy O. Josephson and Jason P. Moore for the sectioning, staining, and imaging of bone samples. We also thank Dr. Lamya Karim and Taraneh Rezaee at the University of Massachusetts Dartmouth for providing and cutting the cortical bone samples. We further thank Dr. Theresa A. Freeman for providing us with the laboratory facilities of Thomas Jefferson University. We also thank Mr. Amirreza Sadighi for his helpful comments on the manuscript writing style.

**Funding** This study was supported by faculty start-up funding from the Department of Mechanical Engineering and Mechanics at Drexel University. The development of the fatigue fracture framework is also supported by the NSF CAREER Award CMMI-2143422.

## Declarations

**Informed consent** N/A.

**Conflict of interest** The authors declare that they have no conflict of interest.

**Human and animal rights and informed consent** This article does not contain any studies with human or animal subjects performed by any

of the authors. All reported studies/experiments with human subjects performed by the authors have been previously published and complied with all applicable ethical standards.

## References


1. Acevedo C, Stadelmann VA, Pioletti DP, Alliston T, Ritchie RO (2018) Fatigue as the missing link between bone fragility and fracture. Nature Biomed Eng 2(2):62–71
2. Lodge CJ, Sha S, Yousef ASE, MacEachern C (2020) Stress fractures in the young adult hip. J Orthop Trauma 34(2):95–100
3. Iwamoto J, Takeda T (2003) Stress fractures in athletes: review of 196 cases. J Orthop Sci 8(3):273–278
4. Meurman K, Elfving S (1980) Stress fracture in soldiers: a multifocal bone disorder. a comparative radiological and scintigraphic study. Radiology 134(2):483–487
5. Breer S, Krause M, Marshall RP, Oheim R, Amling M, Barvencik F (2012) Stress fractures in elderly patients. Int Orthop 36(12):2581–2587
6. Carpintero P, Berral FJ, Baena P, Garcia-Frasquet A, Lancho JL (1997) Delayed diagnosis of fatigue fractures in the elderly. Am J Sports Med 25(5):659–662
7. Colopy S, Benz-Dean J, Barrett J, Sample S, Lu Y, Danova N et al (2004) Response of the osteocyte syncytium adjacent to and distant from linear microcracks during adaptation to cyclic fatigue loading. Bone 35(4):881–891
8. Burr DB, Forwood MR, Fyhrie DP, Martin RB, Schaffler MB, Turner CH (1997) Bone microdamage and skeletal fragility in osteoporotic and stress fractures. J Bone Mineral Res 12(1):6–15
9. Seref-Ferlengez Z, Kennedy OD, Schaffler MB (2015) Bone microdamage, remodeling and bone fragility: how much damage is too much damage? BoneKEy reports 4
10. Nyman JS, Makowski AJ (2012) The contribution of the extracellular matrix to the fracture resistance of bone. Current osteoporos Rep 10(2):169–177
11. Vashishth D (2009) Advanced glycation end-products and bone fractures. Ibms Bonekey 6(8):268
12. Karim L, Bouxsein ML (2016) Effect of type 2 diabetes-related non-enzymatic glycation on bone biomechanical properties. Bone 82:21–27
13. Collier T, Nash A, Birch H, De Leeuw N (2018) Effect on the mechanical properties of type i collagen of intra-molecular lysine-arginine derived advanced glycation end-product cross-linking. J Biomech 67:55–61
14. Merlo K, Aaronson J, Vaidya R, Rezaee T, Chalivendra V, Karim L (2020) In vitro-induced high sugar environments deteriorate human cortical bone elastic modulus and fracture toughness. J Orthop Res 38(5):972–983
15. Saito M, Mori S, Mashiba T, Komatsubara S, Marumo K (2008) Collagen maturity, glycation induced-pentosidine, and mineralization are increased following 3-year treatment with incadronate in dogs. Osteoporos Int 19(9):1343–1354
16. Tang S, Vashishth D (2010) Non-enzymatic glycation alters microdamage formation in human cancellous bone. Bone 46(1):148–154
17. Nguyen HQ, Nguyen TNT, Pham TQD, Nguyen VD, Tran XV, Dao TT (2021) Crack propagation in the tibia bone within total knee replacement using the extended finite element method. Appl Sci 11(10):4435
18. Kahla RB, Barkaoui A, Merzouki T (2018) Age-related mechanical strength evolution of trabecular bone under fatigue damage for both genders: Fracture risk evaluation. J Mech Behav Biomed Mater 84:64–73
19. Hambli R, Hattab N (2013) Application of neural network and finite element method for multiscale prediction of bone fatigue crack growth in cancellous bone. Multiscale Computer Modeling in Biomechanics and Biomedical Engineering 3–30
20. Waanders D, Janssen D, Miller MA, Mann KA, Verdonschot N (2009) Fatigue creep damage at the cement-bone interface: an experimental and a micro-mechanical finite element study. J Biomech 42(15):2513–2519
21. Nguyen TT, Yvonnet J, Zhu QZ, Bornert M, Chateau C (2015) A phase field method to simulate crack nucleation and propagation in strongly heterogeneous materials from direct imaging of their microstructure. Eng Fract Mech 139:18–39
22. Remmers JJ, de Borst R, Needleman A (2008) The simulation of dynamic crack propagation using the cohesive segments method. J Mech Phys Solids 56(1):70–92
23. Moës N, Dolbow J, Belytschko T (1999) A finite element method for crack growth without remeshing. Int J Num Methods Eng 46(1):131–150
24. Ghorashi SS, Valizadeh N, Mohammadi S, Rabczuk T (2015) T-spline based xiga for fracture analysis of orthotropic media. Comput Struct 147:138–146
25. Natarajan S, Annabattula RK, Martínez-Pañeda E et al (2019) Phase field modelling of crack propagation in functionally graded materials. Compos Part B: Eng 169:239–248
26. Ambati M, Gerasimov T, De Lorenzis L (2015) Phase-field modeling of ductile fracture. Comput Mech 55(5):1017–1040
27. Miehe C, Hofacker M, Welschinger F (2010) A phase field model for rate-independent crack propagation: robust algorithmic implementation based on operator splits. Comput Methods Appl Mech Eng 199(45–48):2765–2778
28. Wu JY, Nguyen VP, Nguyen CT, Sutula D, Bordas S, Sinaie S (2018) Phase field modeling of fracture. Advances in applied mechancis: multi-scale theory and computation 52
29. de Borst R, Verhoosel CV (2016) Gradient damage vs phase-field approaches for fracture: similarities and differences. Comput Methods Appl Mech Eng 312:78–94
30. Goswami S, Anitescu C, Chakraborty S, Rabczuk T (2020) Transfer learning enhanced physics informed neural network for phase-field modeling of fracture. Theor Appl Fract Mech 106:102447
31. Msekh MA, Cuong N, Zi G, Areias P, Zhuang X, Rabczuk T (2018) Fracture properties prediction of clay/epoxy nanocomposites with interphase zones using a phase field model. Eng Fract Mech 188:287–299
32. Maghami E, Moore JP, Josephson TO, Najafi AR (2022) Damage analysis of human cortical bone under compressive and tensile loadings. Comput Methods Biomech Biomed Eng 25(3):342–357
33. Josephson TO, Moore JP, Maghami E, Freeman TA, Najafi AR (2022) Computational study of the mechanical influence of lacunae and perilacunar zones in cortical bone microcracking. J Mech Behav Biomed Mater 126:105029
34. Maghami E, Josephson TO, Moore JP, Rezaee T, Freeman TA, Karim L et al (2021) Fracture behavior of human cortical bone: role of advanced glycation end-products and microstructural features. J Biomech 125:110600
35. Maghami E, Pejman R, Najafi AR (2021) Fracture micromechanics of human dentin: a microscale numerical model. J Mech Behav Biomed Mater 114:104171
36. Nguyen L, Stoter S, Baum T, Kirschke J, Ruess M, Yosibash Z et al (2017) Phase-field boundary conditions for the voxel finite cell method: surface-free stress analysis of ct-based bone structures. Int J Numer Methods Biomed Eng 33(12):e2880
37. Maghami E, Najafi AR (2022) Influence of age-related changes on crack growth trajectories and toughening mechanisms in human dentin. Dent Mater 38(11):1789–1800

38. Wu C, Fang J, Zhang Z, Entezari A, Sun G, Swain MV et al (2020) Fracture modeling of brittle biomaterials by the phase-field method. Eng Fract Mech 224:106752
39. Pinto DC, Pace ED (2015) A silver-stain modification of standard histological slide preparation for use in anthropology analyses. J Forensic Sci 60(2):391–398
40. Gustafsson A, Khayyeri H, Wallin M, Isaksson H (2019) An interface damage model that captures crack propagation at the microscale in cortical bone using xfem. J Mech Behav Biomed Mater 90:556–565
41. Saffar KP, Najafi AR, Moeinzadeh MH, Sudak LJ (2013) A finite element study of crack behavior for carbon nanotube reinforced bone cement. World J Mech 3(5A):13–21
42. Abdel-Wahab AA, Maligno AR, Silberschmidt VV (2012) Micro-scale modelling of bovine cortical bone fracture: analysis of crack propagation and microstructure using x-fem. Comput Mater Sci 52(1):128–135
43. Fan Z, Swadener J, Rho J, Roy M, Pharr G (2002) Anisotropic properties of human tibial cortical bone as measured by nanoindentation. J Orthop Res 20(4):806–810
44. Fratzl P, Gupta H, Paschalis E, Roschger P (2004) Structure and mechanical quality of the collagen-mineral nano-composite in bone. J Mater Chem 14(14):2115–2123
45. Giner E, Belda R, Arango C, Vercher-Martínez A, Tarancón JE, Fuenmayor FJ (2017) Calculation of the critical energy release rate gc of the cement line in cortical bone combining experimental tests and finite element models. Eng Fract Mech 184:168–182
46. Brown CU, Yeni YN, Norman TL (2000) Fracture toughness is dependent on bone location–a study of the femoral neck, femoral shaft, and the tibial shaft. J Biomed Mater Res: Off J Soc Biomater Jpn Soc Biomater 49(3):380–389
47. Tang S, Vashishth D (2011) The relative contributions of non-enzymatic glycation and cortical porosity on the fracture toughness of aging bone. J Biomech 44(2):330–336
48. Bourdin B, Francfort GA, Marigo JJ (2008) The variational approach to fracture. J Elast 91(1–3):5–148
49. Kristensen PK, Martínez-Pañeda E (2020) Phase field fracture modelling using quasi-newton methods and a new adaptive step scheme. Theor Appl Fract Mech 107:102446
50. Alessi R, Vidoli S, De Lorenzis L (2018) A phenomenological approach to fatigue with a variational phase-field model: the one-dimensional case. Eng Fract Mech 190:53–73
51. Carrara P, Ambati M, Alessi R, De Lorenzis L (2020) A framework to model the fatigue behavior of brittle materials based on a variational phase-field approach. Comput Methods Appl Mech Eng 361:112731
52. Burr DB (2019) Changes in bone matrix properties with aging. Bone 120:85–93
53. Li J, Gong H (2021) Fatigue behavior of cortical bone: a review. Acta Mech Sinica 37(3):516–526
54. Varvani-Farahani A, Najmi H (2010) A damage assessment model for cadaveric cortical bone subjected to fatigue cycles. Int J Fatigue 32(2):420–427
55. Taylor D (2018) Observations on the role of fracture mechanics in biology and medicine. Eng Fract Mech 187:422–430
56. Wegst UG, Bai H, Saiz E, Tomsia AP, Ritchie RO (2015) Bioinspired structural materials. Nature Mater 14(1):23–36
57. Carter D, Hayes WC, Schurman DJ (1976) Fatigue life of compact bone–ii. effects of microstructure and density. J Biomech 9(4):211-218
58. Poundarik AA, Wu PC, Evis Z, Sroga GE, Ural A, Rubin M et al (2015) A direct role of collagen glycation in bone fracture. J Mech Behav Biomed Mater 52:120–130
59. Carando S, Barbos MP, Ascenzi A, Boyde A (1989) Orientation of collagen in human tibial and fibular shaft and possible correlation with mechanical properties. Bone 10(2):139–142
60. Mischinski S, Ural A (2013) Interaction of microstructure and microcrack growth in cortical bone: a finite element study. Comput Methods Biomech Biomed Eng 16(1):81–94
61. Budyn E, Hoc T, Jonvaux J (2008) Fracture strength assessment and aging signs detection in human cortical bone using an x-fem multiple scale approach. Comput Mech 42(4):579–591
62. Li S, Abdel-Wahab A, Demirci E, Silberschmidt VV (2014) Fracture process in cortical bone: X-fem analysis of microstructured models. In: Fracture phenomena in nature and technology Springer, pp 43–55




**Ebrahim Maghami** is a PhD candidate in mechanical engineering at Drexel University. His research is on computational crack growth simulation and numerical damage modeling in biological tissues.

**Dr. Ahmad R. Najafi** is Assistant Professor at Drexel University and works on numerical optimization, bio-inspired design, and computational modeling of the damage mechanisms of biological materials.